FROM DISCRETE ELEMENT SIMULATIONS TOWARDS A CONTINUUM DESCRIPTION OF PARTICULATE SOLIDS

Stefan Luding, Marc Lätzel, and Hans J. Herrmann

Institute for Computer Applications 1,
Pfaffenwaldring 27, 70569 Stuttgart, Germany
e-mail: lui@ica1.uni-stuttgart.de
web-page: http://www.ica1.uni-stuttgart.de/

Abstract – We propose a way to obtain averaged macroscopic quantities like density, momentum flux, stress, and strain from "microscopic" numerical simulations of particles in a two-dimensional ring-shear-cell. In the steady-state, a shear zone is found, about six particle diameters wide, in the vicinity of the inner, moving wall. The velocity decays exponentially in the shear zone, particle rotations are observed, and the stress and strain-tensors are highly anisotropic and, even worse, not co-linear. From combinations of the tensorial quantities, one can obtaini, for example, the bulk-stiffness of the granulate and its shear modulus.

1. INTRODUCTION

The description of the behavior of particulate materials relies on constitutive equations, functions of stress, strain, and other physical quantities describing the system. It is rather difficult to extract macroscopic observables like the stress from experiments, e.g. in a two-dimensional (2D) geometry with photo-elastic material, where stress is visualized via crossed polarizers [6, 7]. The alternative is, to perform discrete element simulations [2, 4] and to average over the *microscopic* quantities in the simulation, in order to obtain some averaged *macroscopic* quantity. The averages over scalar quantities like density, velocity and particle-spin are straightforward, but for the stress and the deformation gradient, one finds slightly different definitions in the literature [3, 8-11].

In the following, we will briefly introduce the boundary conditions for our model system, before presenting the averaging procedure. Kinematic and dynamic quantities of the system are obtained from the simulation data and some material properties are determined as combinations of the observables.

2. MODEL AND AVERAGING STRATEGY

In the following, a two-dimensional (2D) Couette-shear-cell is used, filled with bidisperse disks of diameter d and height h, a snapshot of the system is displayed in Fig. 1. The system is slowly sheared by turning the inner ring counter-clockwise about once per minute.
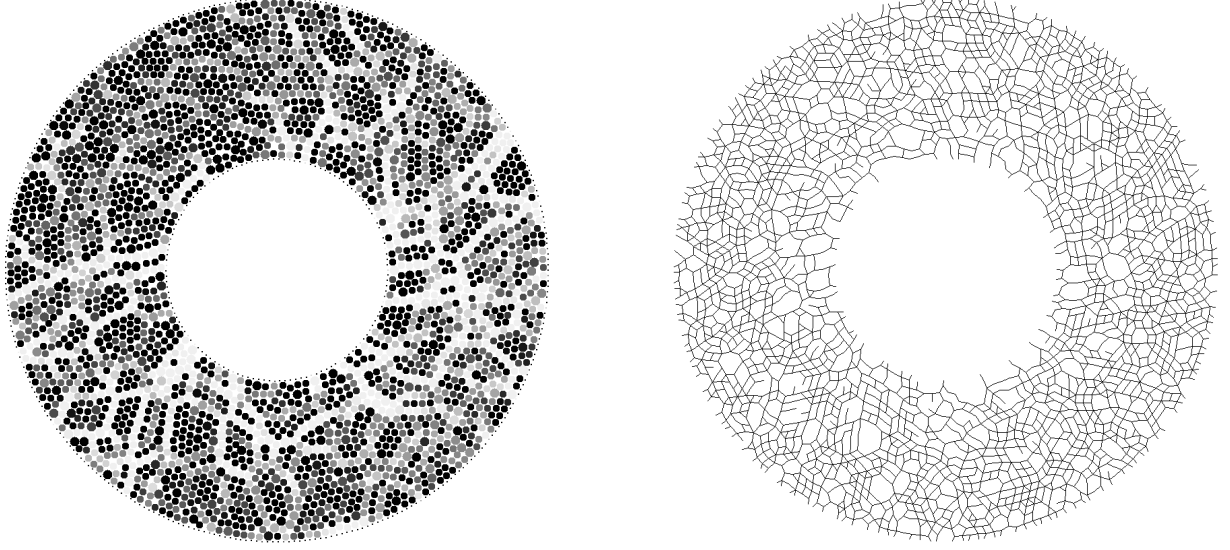
Fig. 1: Snapshot from the model system. (Left) Stress chains - dark particles feel low pressure, light particles are strongly compressed. (Right) Contact network - each contact is plotted as a line.

The inner and the outer ring have a radius of R_i=0.1034 m and R_o=0.2526 m, respectively. In the experiment, the height of the system is h=0.006 m and it is filled with slightly smaller disks of diameters d_s =7.42 mm and d_l=8.99 mm, in order to avoid crystalization. The results presented in this study stem from three simulation with $N=N_s+N_l$ particles. These simulations, referred to as (1), (2), and (3) in the following, with $N_{(1)}$=2555 +399, $N_{(2)}$=2545+394, and $N_{(3)}$=2511+400, correspond to an area coverage, or volume fraction of $v_{(1)}$=0.8194, $v_{(2)}$=0.8149, and $v_{(3)}$=0.8084, respectively. The angular frequency of the inner ring is $\Omega=2\pi/T$=0.1s^{-1} and the simulation is performed until t=120s; for the averaging, the first rotation is disregarded. For more details see Ref. [9].

The averaging procedure, as applied in the following, can be formalized for any quantity Q, keeping in mind that we first average over each particle and then attribute a fraction of each particle – and thus a fraction of Q – to the corresponding averaging volume. An alternative approach, i.e. to use the fraction of the center-center line of the particles instead of the volume [5], is not applied here. Written as a formula our ansatz reads

$$Q = \left\langle Q^p \right\rangle = \frac{1}{V} \sum_{p \in V} w_V^p V^p Q^p, \quad \text{with} \quad Q^p = \sum_{c=1}^{C^p} Q^c, \tag{1}$$

where Q^p is the pre-averaged particle quantity and Q^c the fraction attributed to contact c of particle p which has C^p contacts. The factor w_V^p is the weight corresponding to the fraction of the particle volume V^p which lies inside the averaging volume V. Due to the symmetry of the system, rings at radial distance r from the center and width Δr can be used, so that $V=2\pi hr\Delta r$. The first important quantity to measure is the volume fraction

$$v = \frac{1}{V} \sum_{p \in V} w_V^p V^p, \tag{2}$$

obtained by using Q^p=1, and disregarding the sum over the contacts. The volume fraction is related to the mass density via $\rho(r)= \rho^p v$, with the material's density ρ^p=1060 kg m^{-3}, paralleling the experiments [6, 7, 9]. The next quantity of interest is the mean momentum flux density

$$v\mathbf{v} = \frac{1}{V} \sum_{p \in V} w_V^p V^p \mathbf{v}^p, \tag{3}$$

obtained with $Q^p=\mathbf{v}^p$, the velocity of particle p. We checked that v$_r$, the radial component of the velocity vector, is approximately zero, in accordance with the assumption of a steady state

cylindrical shear situation. In Fig. 2, the density ν and the velocity v_ϕ are plotted against the distance from the center r.
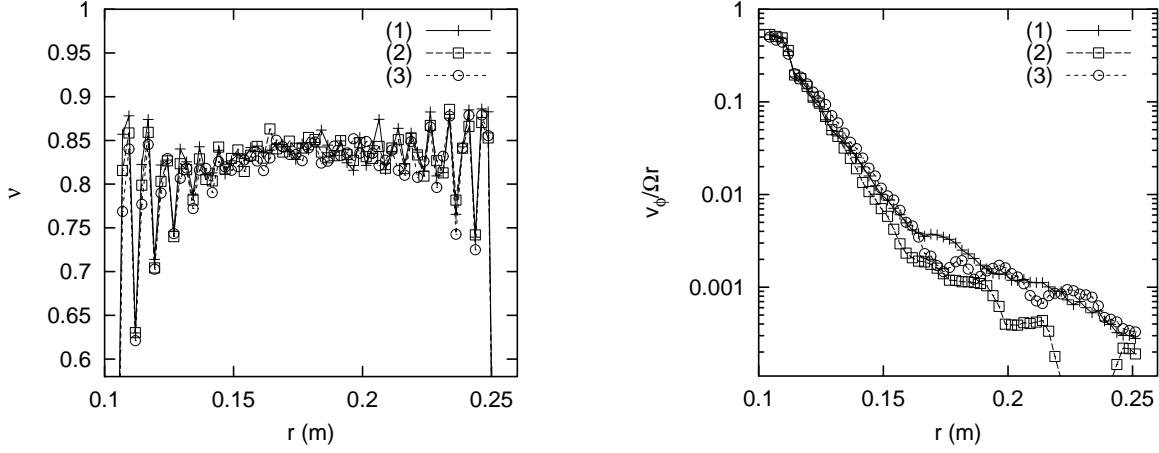

Fig. 2: Snapshot (Left) Density ν and (Right) scaled tangential velocity $v_\phi/\Omega r$, with the angular velocity Ωr of a solid body rotating with the inner ring, plotted against the distance from the center r. The different symbols and lines correspond to different densities and we used 60 intervals for binning, here.

We identify the shear zone with those parts of the system with large v_ϕ. Like in the experiments, the material is dilated in the shear-zone near the inner, rotating wall and also in the vicinity of the outer boundary, whereas it is densified in the central part (due to mass conservation and the fixed volume boundary conditions). Particles are layered close to the walls, as indicated by the periodic wiggles in density, but no order effects are visible in the inner parts of the system. The velocity decays exponentially from the inner ring over two orders of magnitude, before it reaches some noise-level. The qualitative picture does not vary with the density; however, if the density would be reduced further below the value of simulation (3), the innermost particles would lose contact with the moving inner wall and the system would freeze.

3. FABRIC, STRESS AND ELASTIC DEFORMATION

The fabric tensor, which describes the directed probability distributio to find a contact, involves the contact normal vectors $\mathbf{n}^c$, related to the so-called branch vectors $\mathbf{l}^{pc}=(d^p/2)\,\mathbf{n}^c$ from the center of particle p with diameter d^p to its contact c, so that

$$\mathbf{F} = \frac{1}{V}\sum_{p\in V} w_V^p V^p \sum_{c=1}^{C^p} \mathbf{n}^c \otimes \mathbf{n}^c \qquad (4)$$

when using $V^p = \pi h(d^p/2)^2$. The tensor $\mathbf{F}$ is normalized so that its trace $\mathrm{tr}(\mathbf{F})=\nu C$, with the mean coordination number C. The deviator of the fabric is a measure for the anisotropy of the contact network [9].

The static component of the stress tensor [8, 9] is defined as the dyadic product of the force $\mathbf{f}^c$ acting at contact c with the corresponding branch vector, where every contact contributes with ist force and its branch vector, if the particle lies in the averaging volume

$$\underline{\underline{\sigma}} = \frac{1}{V}\sum_{p\in V} w_V^p \sum_{c=1}^{C^p} \mathbf{f}^c \otimes \mathbf{l}^{pc}, \qquad (5)$$

and the dynamic component of the stress tensor,

$$^d\underline{\underline{\sigma}} = \frac{1}{V}\sum_{p\in V} w_V^p V^p \rho^p \mathbf{v}^p \otimes \mathbf{v}^p, \qquad (6)$$

has two contributions: (i) the stress due to velocity fluctuations around the mean and (ii) a stress due to the mean mass transport in angular direction. In Fig. 3, the static and the dynamic contributions are plotted. In our system, the diagonal elements of the static stress are almost constant, whereas the off-diagonal elements decay proportional to r^{-2}. The angular velocity in the shear zone strongly contributes to the stress due to mass flux, however, the dynamic stress is usually much smaller than the static stress.
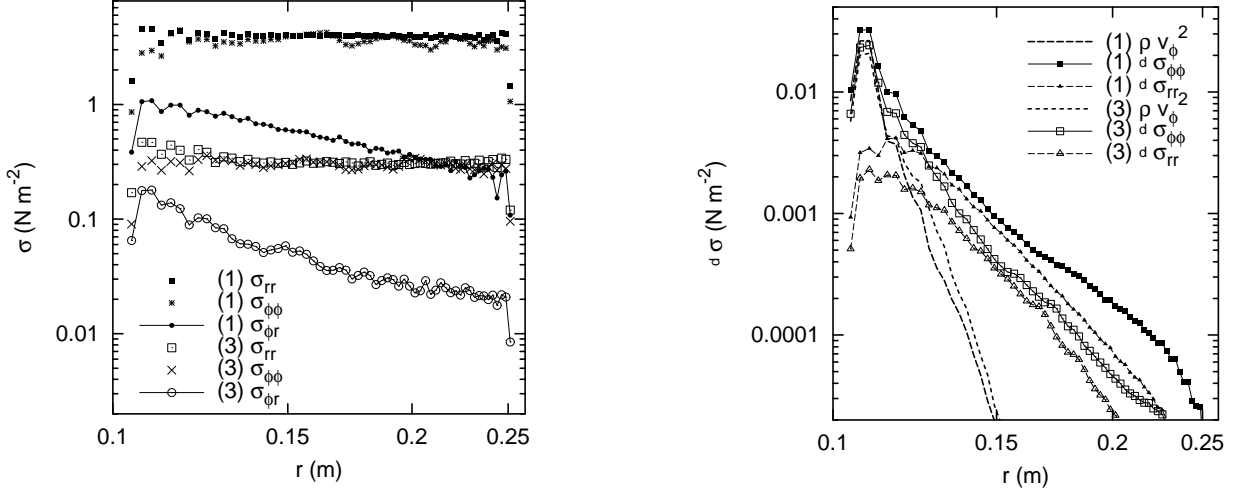

Fig. 3: Components of the static stress (Left) and the dynamic stress (Right), and the fluctuation contribution ρv_ϕ^2, plotted against the distance from the center r. Note the different vertical axis scaling. Only the dense simulation (1), solid symbols, is compared to the dilute one (3), open symbols.

Finally, the elastic deformation gradient [9,10] is defined as

$$\underline{\underline{\varepsilon}} = \frac{\pi h}{V}\left(\sum_{p\in V} w_V^p \sum_{c=1}^{C^p} \Delta^{pc}\otimes \mathbf{l}^{pc}\right)\cdot \mathbf{A}\,, \qquad (7)$$

where $\Delta^{pc}=\delta^c \mathbf{n}^c$ is the deformation vector of contact c, with the deformation δ^c, and $\mathbf{A}=\mathbf{F}^{-1}$ is the inverse fabric tensor. The elastic deformation gradient is a measure for the mean reversible deformation of the material and thus for the energy stored in the compressed granulate. In the following, we extract some material properties from the quantities defined above.

In Fig. 4 the rescaled stiffness and some shear modulus of the granulate are plotted against the trace of the fabric. Furthermore, the orientations of the tensors $\mathbf{F}$, σ, and ε are plotted against the distance from the inner ring. The data for the bulk modulus from different simulations collapse on a master curve, except for the areas close to the walls. The data for the shear modulus show a non-linear increase with $\mathrm{tr}(\mathbf{F})$; the denser system diverges at larger values than the dilute system, however, the data are strongly scattered. The most remarkable result is the fact that the orientations ϕ_T of the tensors are not co-linear, where ϕ_T is defined as the orientation of the "major eigenvector", i.e. the eigenvector corresponding to the major eigenvalue of T, with respect to the radial direction.

In Fig. 5, the mean total particle spin, ω, as obtained from the spin density

$$v\omega = \frac{1}{V}\sum_{p\in V} w_V^p V^p \omega^p\,, \qquad (8)$$

is plotted, together with the continuum spin $W_{r\phi}$ and the excess or eigen-spin, $\omega^*=\omega - W_{r\phi}$, as functions of r in the few innermost layers. We remark that the rotation of the particles is a stable effect, independent of the density, at least in the range of densities examined here. The particles in the innermost layer rotate clockwise and in the next layer, a counter-clockwise spin is evidenced; the particles in the innermost sheared layers roll over each other.

Note that both the deformation rate $D_{r\phi}$ and the continuum spin $W_{r\phi}$ are obtained by addition and subtraction, respectively, of the velocity gradient's off-diagonal elements

$$\left[\nabla\mathbf{v}\right]_{r\phi} = \frac{\partial \mathrm{v}_\phi}{\partial r}, \quad \text{and} \quad \left[\nabla\mathbf{v}\right]_{\phi r} = -\frac{\mathrm{v}_\phi}{r}, \tag{8}$$

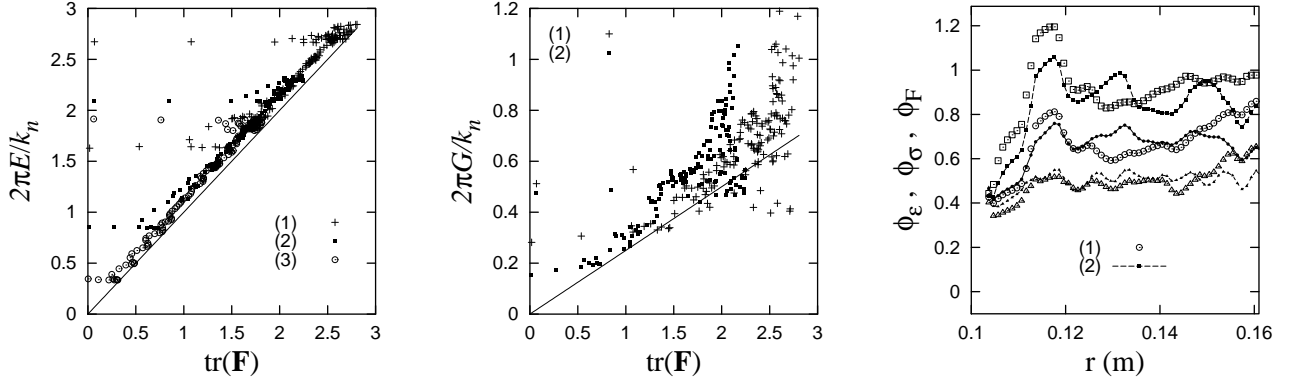where we compute the partial derivative with respect to r from the data of v_ϕ directly.

Fig. 4: (Left) Granulate stiffness $2\pi E/k_\mathrm{n}=\mathrm{tr}(\sigma)/\mathrm{tr}(\varepsilon)$, plotted against $\mathrm{tr}(\mathbf{F})$. (Middle) Scaled granulate shear resistance $2\pi G/k_\mathrm{n}=\mathrm{dev}(\sigma)/\mathrm{dev}(\varepsilon)$, plotted against $\mathrm{tr}(\mathbf{F})$. (Right) Orientation of the fabric-, stress-, and strain-tensors (from top to bottom). Here 150 binning intervals are used.
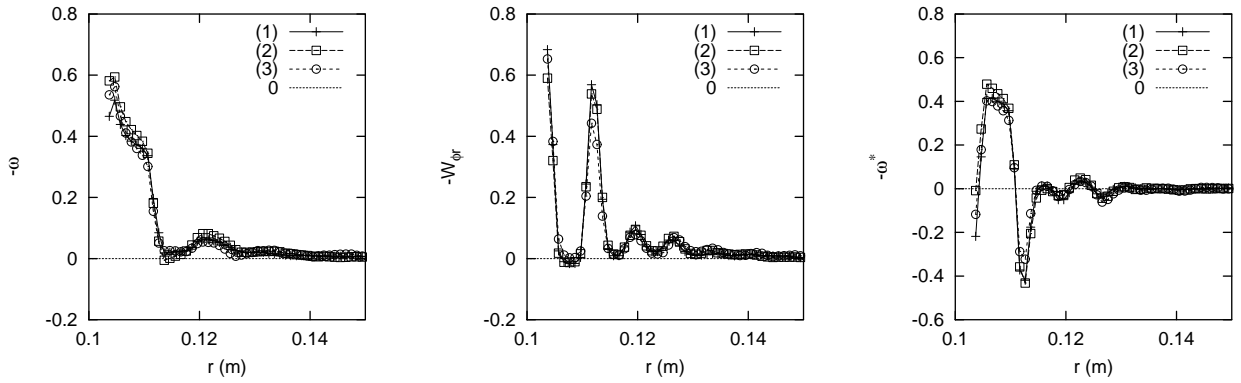

Fig. 5: (Left) Total particle spin ω, which consists of the contiuum spin $W_{r\phi}$ (Middle) and an excess eigen-spin ω^* (Right). Different symbols correspond to different densities; 150 binning intervals are used.

4. DISCUSSION

In summary, we used numerical simulations of disks in a shear-cell and obtained kinematic and dynamic quantities by averaging over rings around the center. In agreement with experiments, a shear-zone with exponentially decaying shear velocity is observed at the inner, moving wall. Ahead with shear goes some dilation of the material and alternating eigen-rotation of the particles.

One also observes that the isotropic parts of fabric, stress and strain are connected via the material's bulk modulus which is proportional to the coordination number density, i.e. the trace of the fabric tensor multiplied by the volume fraction. In a similar picture, the shear modulus shows non-linear behavior, a divergence at large contact densities, and strong scatter, all indicating additional effects not accounted for by an isotropic elastic theory. Furthermore, the stress-, strain- and fabric tensors are *not co-linear*, i.e. the material is an-isotropic and thus cannot be described by a classical isotropic elasticity theory and only two material paramters.

Understanding the connection between stress and strain and the influence of an anisotropic fabric is subject of current research. Furthermore, we study the influence of static friction and other microscopic material parameters on the physics of the shear-cell. In addition, the connection

between the shear and the particle eigen-rotations is an open issue in the framework of a micro-polar description.

5. REFERENCES

1. R. J. Bathurst and L. Rothenburg, Micromechanical aspects of isotropic granular assemblies with linear contact interactions. *J. Appl. Mech.* **55**, 17, 1988.
2. P. A. Cundall and O. D. L. Strack, A discrete numerical model for granular assemblies. *Géotechnique*, **29**(1), 47, 1979.
3. J. D. Goddard, Continuum Modeling of Granular Assemblies, in [4].
4. I. Goldhirsch, Note on the definition of stress for discrete systems. *preprint* (1999).
5. H. J. Herrmann, J.-P. Hovi, and S. Luding, editors, *Physics of dry granular media* - NATO ASI Series E 350. Kluwer Academic Publishers, Dordrecht, 1998.
6. D. W. Howell and R. P. Behringer, Fluctuations in a 2D granular Couette experiment: A critical transition, *Phys. Rev. Lett.* **82**, 5241, 1999.
7. D. W. Howell, R. P. Behringer, and C. T. Veje, Fluctuations in granular media, *Chaos* **9**, 559, 1999.
8. N. P. Kruyt and L. Rothenburg, Micromechanical definition of strain tensor for granular materials. *ASME Journal of Applied Mechanics* **118**, 706, 1996.
9. M. Lätzel, S. Luding, and H. J. Herrmann, Macroscopic material properties from quasi-static, microscopic simulations of a two-dimensional shear-cell. *Granular Matter* **2**(3), in press, 2000.
10. C.-L. Liao, T.-P. Chang, D.-H. Young, and C. S. Chang, Stress-strain relationship for granular materials based on the hypothesis of best fit. *Int. J. Solids Structures* **34**, 4087, 1997.
11. S. B. Savage and D. J. Jeffrey, The stress tensor in a granular flow at high shear rates. *J. Fluid. Mech.*, **110**, 255, 1981.

6. ACKNOWLEDGEMENTS